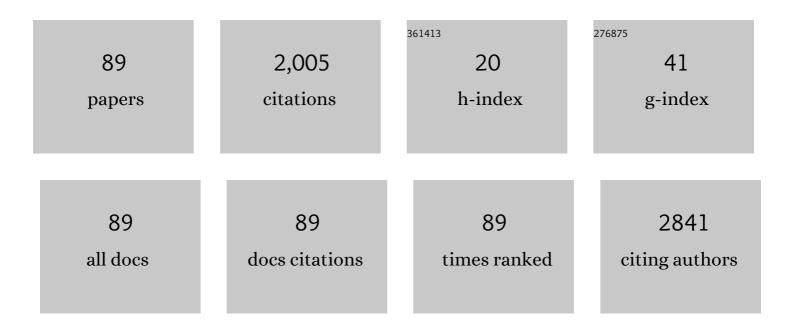
Daniel B Ennis

List of Publications by Year in descending order

Source: https://exaly.com/author-pdf/1165733/publications.pdf Version: 2024-02-01



#	Article	IF	CITATIONS
1	Orthogonal tensor invariants and the analysis of diffusion tensor magnetic resonance images. Magnetic Resonance in Medicine, 2006, 55, 136-146.	3.0	242
2	Assessment of Myocardial Microstructural Dynamics by InÂVivo Diffusion Tensor Cardiac Magnetic Resonance. Journal of the American College of Cardiology, 2017, 69, 661-676.	2.8	171
3	Modelling passive diastolic mechanics with quantitative MRI of cardiac structure and function. Medical Image Analysis, 2009, 13, 773-784.	11.6	155
4	Pacemaker lead tip heating in abandoned and pacemakerâ€attached leads at 1.5 tesla MRI. Journal of Magnetic Resonance Imaging, 2011, 33, 426-431.	3.4	123
5	Device artifact reduction for magnetic resonance imaging of patients with implantable cardioverter-defibrillators and ventricular tachycardia: Late gadolinium enhancement correlation with electroanatomic mapping. Heart Rhythm, 2014, 11, 289-298.	0.7	86
6	Convex optimized diffusion encoding (<scp>CODE</scp>) gradient waveforms for minimum echo time and bulk motion–compensated diffusionâ€weighted <scp>MRI</scp> . Magnetic Resonance in Medicine, 2017, 77, 717-729.	3.0	82
7	The presence of two local myocardial sheet populations confirmed by diffusion tensor MRI and histological validation. Journal of Magnetic Resonance Imaging, 2011, 34, 1080-1091.	3.4	69
8	Diffusion Tensor Analysis With Invariant Gradients and Rotation Tangents. IEEE Transactions on Medical Imaging, 2007, 26, 1483-1499.	8.9	63
9	Visualization of tensor fields using superquadric glyphs. Magnetic Resonance in Medicine, 2005, 53, 169-176.	3.0	60
10	Construction and Validation of Subject-Specific Biventricular Finite-Element Models of Healthy and Failing Swine Hearts From High-Resolution DT-MRI. Frontiers in Physiology, 2018, 9, 539.	2.8	56
11	Simulation Methods and Validation Criteria for Modeling Cardiac Ventricular Electrophysiology. PLoS ONE, 2014, 9, e114494.	2.5	48
12	Scar voltage threshold determination using ex vivo magnetic resonance imaging integration in a porcine infarct model: Influence of interelectrode distances and three-dimensional spatial effects of scar. Heart Rhythm, 2016, 13, 1993-2002.	0.7	39
13	Eddy current–nulled convex optimized diffusion encoding (EN ODE) for distortionâ€free diffusion tensor imaging with short echo times. Magnetic Resonance in Medicine, 2018, 79, 663-672.	3.0	30
14	Noninvasive measurement of myocardial tissue volume change during systolic contraction and diastolic relaxation in the canine left ventricle. Magnetic Resonance in Medicine, 2006, 55, 484-490.	3.0	27
15	Myofiber angle distributions in the ovine left ventricle do not conform to computationally optimized predictions. Journal of Biomechanics, 2008, 41, 3219-3224.	2.1	27
16	Probing dynamic myocardial microstructure with cardiac magnetic resonance diffusion tensor imaging. Journal of Cardiovascular Magnetic Resonance, 2014, 16, 89.	3.3	27
17	Endocardial versus epicardial electrical synchrony during LV free-wall pacing. American Journal of Physiology - Heart and Circulatory Physiology, 2003, 285, H1864-H1870.	3.2	26
18	Testing Foundations of Biological Scaling Theory Using Automated Measurements of Vascular Networks. PLoS Computational Biology, 2015, 11, e1004455.	3.2	24

#	Article	IF	CITATIONS
19	Cardiac MRI biomarkers for Duchenne muscular dystrophy. Biomarkers in Medicine, 2018, 12, 1271-1289.	1.4	24
20	Terahertz Imaging of Cutaneous Edema: Correlation With Magnetic Resonance Imaging in Burn Wounds. IEEE Transactions on Biomedical Engineering, 2017, 64, 2682-2694.	4.2	22
21	Microstructural Infarct Border Zone Remodeling in the Post-infarct Swine Heart Measured by Diffusion Tensor MRI. Frontiers in Physiology, 2018, 9, 826.	2.8	22
22	Highly accelerated, modelâ€free diffusion tensor <scp>MRI</scp> reconstruction using neural networks. Medical Physics, 2019, 46, 1581-1591.	3.0	22
23	Intra-myocardial alginate hydrogel injection acts as a left ventricular mid-wall constraint in swine. Acta Biomaterialia, 2020, 111, 170-180.	8.3	22
24	Fully-automated global and segmental strain analysis of DENSE cardiovascular magnetic resonance using deep learning for segmentation and phase unwrapping. Journal of Cardiovascular Magnetic Resonance, 2021, 23, 20.	3.3	21
25	Quantifying precision in cardiac diffusion tensor imaging with secondâ€order motionâ€compensated convex optimized diffusion encoding. Magnetic Resonance in Medicine, 2018, 80, 1074-1087.	3.0	20
26	Changes in Mitral Annular Geometry and Dynamics With β-Blockade in Patients With Degenerative Mitral Valve Disease. Circulation: Cardiovascular Imaging, 2010, 3, 687-693.	2.6	19
27	Electrophysiology of Heart Failure Using a Rabbit Model: From the Failing Myocyte to Ventricular Fibrillation. PLoS Computational Biology, 2016, 12, e1004968.	3.2	19
28	Effect of flowâ€encoding strength on intravoxel incoherent motion in the liver. Magnetic Resonance in Medicine, 2019, 81, 1521-1533.	3.0	19
29	Evaluation of the impact of strain correction on the orientation of cardiac diffusion tensors with in vivo and ex vivo porcine hearts. Magnetic Resonance in Medicine, 2018, 79, 2205-2215.	3.0	18
30	Cardiac MRI: a Translational Imaging Tool for Characterizing Anthracycline-Induced Myocardial Remodeling. Current Oncology Reports, 2016, 18, 48.	4.0	17
31	Method for the unique identification of hyperelastic material properties using fullâ€field measures. Application to the passive myocardium material response. International Journal for Numerical Methods in Biomedical Engineering, 2017, 33, e2866.	2.1	17
32	The dependence of radiofrequency induced pacemaker lead tip heating on the electrical conductivity of the medium at the lead tip. Magnetic Resonance in Medicine, 2012, 68, 606-613.	3.0	16
33	Using synthetic data generation to train a cardiac motion tag tracking neural network. Medical Image Analysis, 2021, 74, 102223.	11.6	16
34	Fourier analysis of STimulated echoes (FAST) for the quantitative analysis of left ventricular twist. Journal of Magnetic Resonance Imaging, 2012, 35, 587-593.	3.4	15
35	Optimal flip angle for high contrast balanced SSFP cardiac cine imaging. Magnetic Resonance in Medicine, 2015, 73, 1095-1103.	3.0	14
36	Estimating Aggregate Cardiomyocyte Strain Using \$In~Vivo\$ Diffusion and Displacement Encoded MRI. IEEE Transactions on Medical Imaging, 2020, 39, 656-667.	8.9	14

#	Article	IF	CITATIONS
37	The effects of noise over the complete space of diffusion tensor shape. Medical Image Analysis, 2014, 18, 197-210.	11.6	13
38	Probing cardiomyocyte mobility with multi-phase cardiac diffusion tensor MRI. PLoS ONE, 2020, 15, e0241996.	2.5	13
39	Reproducibility of global and segmental myocardial strain using cine DENSE at 3ÂT: a multicenter cardiovascular magnetic resonance study in healthy subjects and patients withÂheart disease. Journal of Cardiovascular Magnetic Resonance, 2022, 24, 23.	3.3	13
40	Chemical shiftâ€induced phase errors in phaseâ€contrast MRI. Magnetic Resonance in Medicine, 2013, 69, 391-401.	3.0	11
41	Variable flip angle balanced steadyâ€state free precession for lower SAR or higher contrast cardiac cine imaging. Magnetic Resonance in Medicine, 2014, 71, 1035-1043.	3.0	11
42	Estimating cardiomyofiber strain in vivo by solving a computational model. Medical Image Analysis, 2021, 68, 101932.	11.6	11
43	Microstructurally Anchored Cardiac Kinematics by Combining In Vivo DENSE MRI and cDTI. Lecture Notes in Computer Science, 2017, 10263, 381-391.	1.3	11
44	Left ventricular twist and shear in patients with primary mitral regurgitation. Journal of Magnetic Resonance Imaging, 2015, 42, 400-406.	3.4	10
45	Timeâ€optimized 4D phase contrast MRI with realâ€ŧime convex optimization of gradient waveforms and fast excitation methods. Magnetic Resonance in Medicine, 2019, 82, 213-224.	3.0	10
46	Optimization methods for magnetic resonance imaging gradient waveform design. NMR in Biomedicine, 2020, 33, e4308.	2.8	10
47	Myofiber strain in healthy humans using DENSE and cDTI. Magnetic Resonance in Medicine, 2021, 86, 277-292.	3.0	10
48	On the impact of vessel wall stiffness on quantitative flow dynamics in a synthetic model of the thoracic aorta. Scientific Reports, 2021, 11, 6703.	3.3	10
49	Linear Invariant Tensor Interpolation Applied to Cardiac Diffusion Tensor MRI. Lecture Notes in Computer Science, 2012, 15, 494-501.	1.3	10
50	Convex gradient optimization for increased spatiotemporal resolution and improved accuracy in phase contrast MRI. Magnetic Resonance in Medicine, 2014, 72, 1552-1564.	3.0	9
51	Effect of freeâ€breathing on left ventricular rotational mechanics in healthy subjects and patients with duchenne muscular dystrophy. Magnetic Resonance in Medicine, 2017, 77, 864-869.	3.0	9
52	T1-Mapping and extracellular volume estimates in pediatric subjects with Duchenne muscular dystrophy and healthy controls at 3T. Journal of Cardiovascular Magnetic Resonance, 2020, 22, 85.	3.3	9
53	Myocardial mesostructure and mesofunction. American Journal of Physiology - Heart and Circulatory Physiology, 2022, 323, H257-H275.	3.2	9
54	Velocity reconstruction with nonconvex optimization for lowâ€velocityâ€encoding phaseâ€contrast <scp>MRI</scp> . Magnetic Resonance in Medicine, 2018, 80, 42-52.	3.0	8

#	Article	IF	CITATIONS
55	High-Resolution Ex Vivo Microstructural MRI After Restoring Ventricular Geometry via 3D Printing. Lecture Notes in Computer Science, 2019, 11504, 177-186.	1.3	8
56	It's the little things: On the complexity of planar electrode heating in MRI. NeuroImage, 2019, 195, 272-284.	4.2	8
57	Fast 3 <scp>D</scp> <scp>T</scp> ₂ â€weighted imaging using variable flip angle transition into driven equilibrium (3 <scp>D</scp> <scp>T</scp> ₂ â€ <scp>TIDE</scp>) balanced <scp>SSFP</scp> for prostate imaging at 3 <scp>T</scp> . Magnetic Resonance in Medicine, 2015, 74, 442-451.	3.0	7
58	Motionâ€Induced Signal Loss in In Vivo Cardiac Diffusionâ€Weighted Imaging. Journal of Magnetic Resonance Imaging, 2020, 51, 319-320.	3.4	7
59	Simultaneous measurement of T ₂ and apparent diffusion coefficient (T ₂ +ADC) in the heart with motionâ€compensated spin echo diffusionâ€weighted imaging. Magnetic Resonance in Medicine, 2018, 79, 654-662.	3.0	6
60	Model of Left Ventricular Contraction: Validation Criteria and Boundary Conditions. Lecture Notes in Computer Science, 2019, 11504, 294-303.	1.3	6
61	Offâ€resonance insensitive complementary SPAtial Modulation of Magnetization (ORIâ€CSPAMM) for quantification of left ventricular twist. Journal of Magnetic Resonance Imaging, 2014, 39, 339-345.	3.4	5
62	Intra―and interscan reproducibility using Fourier Analysis of STimulated Echoes (FAST) for the rapid and robust quantification of left ventricular twist. Journal of Magnetic Resonance Imaging, 2014, 39, 463-468.	3.4	5
63	Phaseâ€contrast MRI with hybrid one and twoâ€sided flowâ€encoding and velocity spectrum separation. Magnetic Resonance in Medicine, 2017, 78, 182-192.	3.0	5
64	A gradient optimization toolbox for general purpose timeâ€optimal MRI gradient waveform design. Magnetic Resonance in Medicine, 2020, 84, 3234-3245.	3.0	5
65	Real-time 3T MRI-guided cardiovascular catheterization in a porcine model using a glass-fiber epoxy-based guidewire. PLoS ONE, 2020, 15, e0229711.	2.5	5
66	Evaluation of a Workflow to Define Low Specific Absorption Rate MRI Protocols for Patients With Active Implantable Medical Devices. Journal of Magnetic Resonance Imaging, 2020, 52, 91-102.	3.4	5
67	Arbitrary Point Tracking with Machine Learning to Measure Cardiac Strains in Tagged MRI. Lecture Notes in Computer Science, 2021, 12738, 213-222.	1.3	5
68	Right Ventricular Function and <scp>T1</scp> â€Mapping in Boys With Duchenne Muscular Dystrophy. Journal of Magnetic Resonance Imaging, 2021, 54, 1503-1513.	3.4	5
69	Quantitative assessment of systolic and diastolic left ventricular twist using Fourier Analysis of Stimulated echoes (FAST) and CSPAMM. Journal of Magnetic Resonance Imaging, 2013, 37, 678-683.	3.4	4
70	Velocity encoding with the slice select refocusing gradient for faster imaging and reduced chemical shiftâ€induced phase errors. Magnetic Resonance in Medicine, 2014, 71, 2014-2023.	3.0	4
71	MRI of Patients with Cardiac Implantable Electronic Devices. Current Cardiovascular Imaging Reports, 2019, 12, 1.	0.6	4
72	Prostate diffusion MRI with minimal echo time using eddy current nulled convex optimized diffusion encoding. Journal of Magnetic Resonance Imaging, 2020, 51, 1526-1539.	3.4	4

#	Article	IF	CITATIONS
73	4D Flow MR Imaging to Improve Microwave Ablation Prediction Models: A Feasibility Study in an InÂVivo Porcine Liver. Journal of Vascular and Interventional Radiology, 2020, 31, 1691-1696.e1.	0.5	4
74	Phase contrast MRI with flow compensation view sharing. Magnetic Resonance in Medicine, 2015, 73, 505-513.	3.0	3
75	Freeâ€breathing variable flip angle balanced SSFP cardiac cine imaging with reduced SAR at 3T. Magnetic Resonance in Medicine, 2016, 76, 1210-1216.	3.0	3
76	Time resolved displacement-based registration of in vivo cDTI cardiomyocyte orientations. , 2018, 2018, 474-478.		3
77	Diffusion Biomarkers in Chronic Myocardial Infarction. Lecture Notes in Computer Science, 2021, 12738, 137-147.	1.3	3
78	Injection of gadolinium contrast through pediatric central venous catheters: a safety study. Pediatric Radiology, 2012, 42, 1064-1069.	2.0	2
79	Complementary radial tagging for improved myocardial tagging contrast. Magnetic Resonance in Medicine, 2015, 73, 1432-1440.	3.0	2
80	Analysis of Location-Dependent Cardiomyocyte Branching. Lecture Notes in Computer Science, 2021, , 189-199.	1.3	2
81	A Framework for Evaluating Myocardial Stiffness Using 3D-Printed Heart Phantoms. Lecture Notes in Computer Science, 2021, , 305-314.	1.3	2
82	Validation of cardiac diffusion tensor imaging sequences: A multicentre test–retest phantom study. NMR in Biomedicine, 2022, 35, e4685.	2.8	2
83	In Vivo Super-Resolution Cardiac Diffusion Tensor MRI: A Feasibility Study. Diagnostics, 2022, 12, 877.	2.6	2
84	Probing cardiomyocyte mobility with multi-phase cardiac diffusion tensor MRI. , 2020, 15, e0241996.		0
85	Probing cardiomyocyte mobility with multi-phase cardiac diffusion tensor MRI. , 2020, 15, e0241996.		0
86	Probing cardiomyocyte mobility with multi-phase cardiac diffusion tensor MRI. , 2020, 15, e0241996.		0
87	Probing cardiomyocyte mobility with multi-phase cardiac diffusion tensor MRI. , 2020, 15, e0241996.		0
88	Probing cardiomyocyte mobility with multi-phase cardiac diffusion tensor MRI. , 2020, 15, e0241996.		0
89	Probing cardiomyocyte mobility with multi-phase cardiac diffusion tensor MRI. , 2020, 15, e0241996.		0